


Oxidation at the sub-nanoscale: oxygen adsorption on graphene-supported size-selected Ag clusters†

Federico Loi, ^a Monica Pozzo, ^b Luca Sbuelz, ^a Luca Bignardi, ^a
Paolo Lacovig, ^c Ezequiel Tosi, ^c Silvano Lizzit, ^c Aras Kartouzian, ^d
Ueli Heiz, ^d Dario Alfè ^{be} and Alessandro Baraldi ^{*ac}



The evolution of the aggregation of condensed matter from single atoms to three-dimensional structures represents an important topic in nanoscience, since it contains essential information to achieve tailor-made growth of nanostructured materials. Such an issue is particularly important in the case of the formation of nano-oxides, which have strong potentialities in heterogeneous catalysis reactions. Herein, we show that a low-nuclearity graphene supported Ag cluster (formed by 11 atoms) shows a local AgO₄ configuration, spatial charge distribution and two oxidation states that are similar to those of bulk AgO. This result indicates that bulk oxide conformations can start to develop already for extremely small atomic aggregates (<1 nm), differently from metallic clusters. This local conformation shows the lowest oxygen vacancy formation energy, which affords high efficiency in the ethylene epoxidation reaction with Ag and strongly supports the possibility of incorporating sub-nanometric clusters in important catalytic reactions.

1 Introduction

Periodic ordering of atoms in crystalline structures is a key element to understand the connection between the structure and properties of a material. However, this crucial feature has a strong dependence on the dimensionality of the periodic structure itself. Once the crystal size decreases from tens of nanometers, at which electronic and structural properties are still dominated by the outer crystal plane characteristics,¹ to a sub-nanometer limit, *i.e.*, towards the quasi-zero dimensional limit, the atomic aggregates begin to show peculiar structural arrangements²⁻⁴ with unique stability,⁵ biomedical,⁶ optical,⁷ energy conversion⁸ and magnetic^{9,10} properties, also in the form of alloys.¹¹ Size-selected clusters are of particular interest for catalysis,¹²⁻¹⁷ and electrocatalysis.^{18,19} The precise control of the number of atoms in the cluster can indeed lead to the production of high-performance catalyzers, as reported by Kawawaki *et al.*²⁰ These aggregates, which in the sub-nanometric regime, often display non-crystalline icosahedral or decahedral structures and²¹ show

a behaviour in elementary processes (such as oxidation) that is still unclear and debated. Proper description of the atomic structure becomes even more difficult in the case of oxides, as in the three- and two-dimensional phases wherein they reveal a structural complexity that is higher than that for metals. At the same time, it is not understood yet whether the local geometric configuration and the oxidation state in the nanoclusters are similar or significantly altered with respect to bulk materials.

To address this issue and gain insight into its atomistic behavior, we studied the oxidation of Ag₁₁ nanoclusters (as schematically outlined in Fig. 1) performed at low pressure (10⁻⁹ Torr) and low temperature (20 K). We demonstrate that an Ag : O atomic ratio close to 1 can be reached and that the atomic arrangement in the clusters tends towards a structure with local coordination, electronic properties, and charge states of Ag and O atoms very similar to those of the AgO bulk species. Insights into the evolution of the local properties in response to the varying oxygen densities in the nanocluster are obtained by combining high-resolution X-ray photoelectron spectroscopy (HR-XPS) and first-principles calculations based on density functional theory (DFT).

2 Experimental and theoretical methods

2.1 Sample preparation

A Ru(0001) single crystal was cleaned by repeated cycles of Ar⁺ sputtering and annealing in an O₂ atmosphere between 600 and 1000 K. The residual oxygen was removed by final flash annealing up to 1500 K. Graphene was grown by thermal

^aDepartment of Physics, University of Trieste, Via Valerio 2, 34127 Trieste, Italy.
E-mail: baraldi@elettra.eu

^bDepartment of Earth Sciences, London Centre for Nanotechnology, University College London, Gower Street, London WC1E 6BT, UK

^cElettra Sincrotrone Trieste, AREA Science Park, 34149 Trieste, Italy

^dChair of Physical Chemistry, Chemistry Department & Catalysis Research Center, Technical University of Munich, Lichtenbergstr. 4, Garching D-85748, Germany

^eDipartimento di Fisica Ettore Pancini, Università di Napoli Federico II, Monte S. Angelo, I-80126 Napoli, Italy

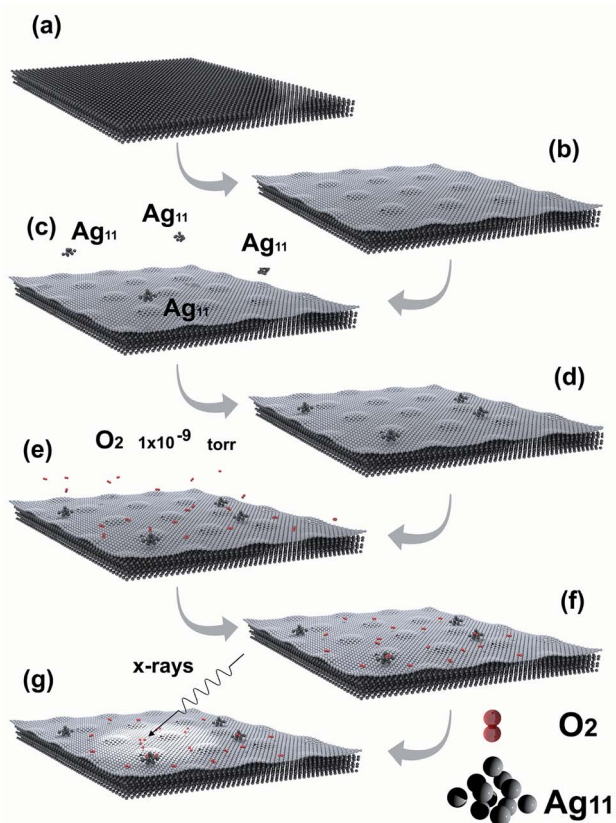


Fig. 1 Outline of the experiment. (a) Clean Ru(0001) substrate; (b) growth of monolayer graphene on Ru(0001); (c) soft-landing of size-selected Ag₁₁ clusters; (d) adsorption of silver clusters; (e) low pressure oxygen exposure at $T = 20$ K; (f) physisorption of O₂ on a silver cluster (and graphene); (g) X-ray (500 eV) induced O₂ dissociation process.

decomposition of ethylene (C₂H₄) at 1100 K. The precursor pressure was initially set to 4×10^{-9} Torr and successively increased in steps up to 4×10^{-8} Torr to ensure that the entire surface was covered with graphene. The resulting graphene layer showed the typical low energy electron diffraction (LEED) pattern with sharp moiré spots^{22,23} (see Fig. 1S of the ESI†).

2.2 Deposition of Ag nanoclusters

Ag₁₁⁺ positive clusters were produced using the cluster source ENAC (exact number of atoms in each cluster). This cluster source is based on the laser ablation of a metal target. The mass selection of clusters is performed with a quadrupole mass analyzer (see Fig. 2S of the ESI†). A more detailed description of the source is reported elsewhere.^{24,25} The Ag₁₁⁺ clusters were deposited on graphene/Ru(0001) (Gr/Ru), on which they are electrically neutralized. The amount of clusters reaching the Gr/Ru surface was monitored by directly reading the current on the sample, on which we applied a positive voltage to reduce the kinetic energy E_k of the clusters, thus ensuring soft landing conditions (*i.e.* $E_k < 1$ eV per atom).^{26,27} The cluster density was below 9×10^{-3} cluster per nm², and the temperature of the sample was kept at 20 K during the deposition, reaction, and measurements to avoid cluster sintering.

2.3 High-resolution X-ray photoelectron spectroscopy

High-resolution X-ray photoelectron spectroscopy (HR-XPS) measurements were performed *in situ* at the SuperESCA beamline of the synchrotron-radiation facility Elettra (Trieste, Italy). The photoemission spectra were collected by means of a Phoibos 150 mm mean-radius hemispherical electron energy analyzer (SPECS), equipped with a delay line detector developed in-house. The overall energy resolution was better than 80 meV for the photon energies and acquisition parameters employed. The XPS spectra were acquired by tuning the photon energy for having a photoelectron kinetic energy of about 100 eV, to enhance a surface sensitivity. For each spectrum, the photoemission intensity was normalized to the photon flux, and the binding energy (BE) scale was aligned to the Fermi level of the Ru(0001) substrate. For the fitting procedure of the core levels, a Doniach-Šunjić²⁸ line profile has been used for each spectral component, convoluted with a Gaussian distribution to account for the experimental, phonon and inhomogeneous broadening. The background was modeled with a second-degree polynomial curve for each Ag 3d_{5/2} spectrum.

2.4 Theoretical methods

Calculations have been carried out using density functional theory (DFT) as implemented in the VASP code.²⁹ The systems were modeled with a slab with 4 layers of Ru in a 12×12 hexagonal supercell and a layer of a 13×13 unit cell of graphene placed on top with an overall number of 914 atoms, excluding the Ag₁₁ cluster. The Ag cluster was placed in the valley of the corrugated graphene layer, with its center on a fcc site, where the stronger interaction with the Ru(0001) substrate increases its stability.³⁰ The bottom two layers of Ru were kept frozen at their bulk geometry, with a lattice parameter of 2.724 Å. The rest of the system was fully relaxed using the rev-vdw-DF2 functional³¹ until the largest residual force was less than 0.015 eV Å⁻¹. We employed the projector augmented method (PAW)³² using PBE³³ potentials. The plane wave cutoff was set to 400 eV, and the relaxations were performed by sampling the Brillouin zone using the Γ point only. To obtain the partial density of states (PDOS), we have performed single point DFT calculations, using geometries obtained with the rev-vdw-DF2 functional. Core-electron BEs have been estimated in the final-state approximation, therefore including also final state effects due to core-hole screening.

3 Results and discussion

For our study, we chose to investigate the oxidation of Ag₁₁, one of the most reactive among the smallest tridimensional Ag clusters. According to the electronic cluster jellium model,^{34,35} it shows an open shell Aufbau configuration $|1S^2|1P^6|1D^3|$, which increases the reactivity of the cluster. Ag clusters display a 3D morphology starting from Ag₈,³⁶ as confirmed by our own DFT calculations, but we selected Ag₁₁ because smaller 3D clusters with an even number of atoms present a lower reactivity,^{36,37} while Ag₉ was excluded due to its electronic similarity to Ag₈, a stable super atom with closed shell configuration $|1S^2|1P^6|$. Ag_{*n*}⁺ mass-selected positive clusters were produced using the

cluster source ENAC^{24,25} and deposited under soft landing conditions on graphene/Ru(0001) (Gr/Ru). Ag-graphene nano-scale heterostructures have been studied in a wide range of fields for their optical,³⁸ catalytic⁷ and antibacterial properties.³⁹ In particular, the experimental study of supported Ag clusters and nanoparticles has been carried out on highly oriented pyrolytic graphite (HOPG), since surface preparation of this system is relatively easy due to its inert surface properties, making it a useful substrate for model systems. The main drawback of using HOPG is the high mobility of nanoclusters at room temperature,⁴⁰ which can be partially overcome by sputter-damaging the surface to create defect sites to stabilize the Ag clusters.⁴¹ However, by doing so, the strong interaction between the clusters and the surface defect can alter the properties of the clusters. To reduce the cluster-substrate interaction and at the same time minimize their mobility to prevent coalescence, we choose the Gr/Ru substrate as a support for the cluster deposition. The adsorption energy of Ag atoms on Gr/Ru being in the range of 20–30 meV (ref. 42–45) is indicative of very weak interaction with graphene; hence, the substrate contribution to the cluster structure and the potential emergence of new properties upon oxidation should be negligible. Moreover, Gr/Ru has already been adopted for the room temperature growth of oxides⁴⁵ since it is a highly corrugated 2D material.⁴⁶ This accounts for a reduced mobility of Ag atoms/clusters, since they tend to remain confined in the depressed region of the carbon network, closer to the metallic substrate.⁴⁷ During the deposition, reaction, and measurement cycles, the temperature was kept at 20 K to prevent Ag cluster sintering, which occurs, for example, when clusters are deposited at room temperature on weakly corrugated surfaces, such as highly oriented pyrolytic graphite.⁴⁰ In addition, the density of clusters on the surface was always kept below 9×10^{-3} cluster per nm², which ensured a statistical occupation of one Ag₁₁ for about 3000 carbon atoms, *i.e. ca.* 9 moiré unit cells of Gr/Ru.

An important issue to address when investigating this system at very low temperature is that the energetic barrier for O₂ dissociation cannot be overcome. Theoretical calculations predict that the presence of dissociated O₂ on a Ag_{*n*} cluster in the gas phase is more favorable than the adsorption of the intact O₂ molecule, already for *n* > 5. Nevertheless, the O₂ dissociation barrier calculated for the clusters seems to be even higher than that for Ag surfaces⁴⁸ (1.11 eV for Ag(111);⁴⁹ 0.36 eV for Ag(110)⁵⁰). Despite the presence of severely under-coordinated atoms in nanoclusters, their oxidation appears more difficult if compared to extended surfaces,⁵¹ hence making the study of the oxidation of Ag nanoclusters very challenging.

In order to achieve complete O₂ dissociation on clusters at very low temperature, we adopted a different strategy relying on the possibility to provide atomic O to foster the oxidation. While the use of plasma-based atomic oxygen beams is well known and employed in several branches of materials science, we decided not to adopt it for this specific study since it has several drawbacks, especially if employed in the low temperature regime: (i) the level of contamination arising from the high background pressure cannot be avoided; (ii) the presence of energetic ions could induce structural modifications in the

cluster morphology and in the substrate. To overcome these difficulties, the Ag₁₁ clusters were exposed to a very low pressure of O₂ at 20 K. Subsequently, the atomic O was obtained by irradiating the clusters covered with physisorbed O₂ with soft X-rays (500 eV) for about 40 minutes. This resulted in an efficient dissociation of the physisorbed O₂ molecules caused by the secondary electrons produced by the photoelectric process.⁵² This procedure based on soft X-ray irradiation was already successfully employed to produce atomic oxygen on both Au foil and nanoparticles,⁵³ on which O₂ does not dissociate spontaneously. The O₂ dissociation on supporting graphene can be observed by inspecting the O 1s core level spectrum, which evolves in time from the characteristic spectrum for gas phase O₂ with two components separated by about 1.12 eV (ref. 53 and 54) into epoxy and enolate species^{55,56} (see O 1s and C 1s spectra in Fig. 3S of the ESI†). However, the spectral contribution coming from the O₂ species physisorbed on the clusters cannot be monitored through the O 1s core level due to the extremely low cluster density. Nevertheless, we were able to observe the oxidation process by measuring the Ag 3d_{5/2} core level.

We acquired spectra for different O₂ exposures after about 40 min of soft X-ray irradiation and analyzed them with the guidance of DFT calculations (Fig. 2(a)–(c)). The oxidation resulted in a 3d_{5/2} core level shift on the cluster towards lower binding energies, confirming the same trend observed for single crystal Ag(111)^{57–59} and Ag(100)^{60–62} surfaces or Ag polycrystalline silver foil⁶³ under high fluxes of atomic oxygen. We also studied the oxidation of the clusters at higher temperature with a dose of 10 L at 70 K (Fig. 4S of the ESI†), and an exposure twenty times that of the maximum dose used at 20 K. This resulted in the Ag 3d spectrum remaining almost unaltered, confirming that the oxidation only occurs due to the soft X-ray induced dissociation of physisorbed molecular O₂. In fact, the O₂ physisorption does not occur at 70 K, which is in line with the extremely small calculated O₂ adsorption energy (0.11 eV). Moreover, the contribution of the reverse spillover at 20 K, *i.e.* the migration of oxygen atoms from the graphene surface to the cluster (which plays a very important role in the case of metal clusters supported on oxides⁶⁴), can be excluded because of the very strong bond between oxygen and carbon atoms of the graphene layer. It is worth comparing our results to the oxidation of larger nanoparticles, of 2.7 and 3.5 nm mean diameter, supported on HOPG, for which a CLS was detected towards higher binding energies upon oxidation.⁶⁵ This CLS was attributed to a final state Coulomb charging related to a shell-like structure of the Ag-nanoparticles with a thin passivating oxide layer and an inner metallic core. This interpretation seems to not apply to the case of our clusters due to their reduced dimensionality. While it is still possible to distinguish between surface and bulk atoms in a nanoparticle of few nanometers, the peculiar structures of matter in the quasi-zero-dimensional limit do not allow for such distinction.^{2–4}

In Fig. 2(d), we report the DFT-calculated Ag 3d_{5/2} core level spectra for the oxidized Ag₁₁O_{2*m*} clusters (*m* = 0–6) that were used to fit the experimental data. We studied only configurations with an even number (2*m*) of O atoms because atomic oxygen is produced from O₂ physisorbed molecules. DFT

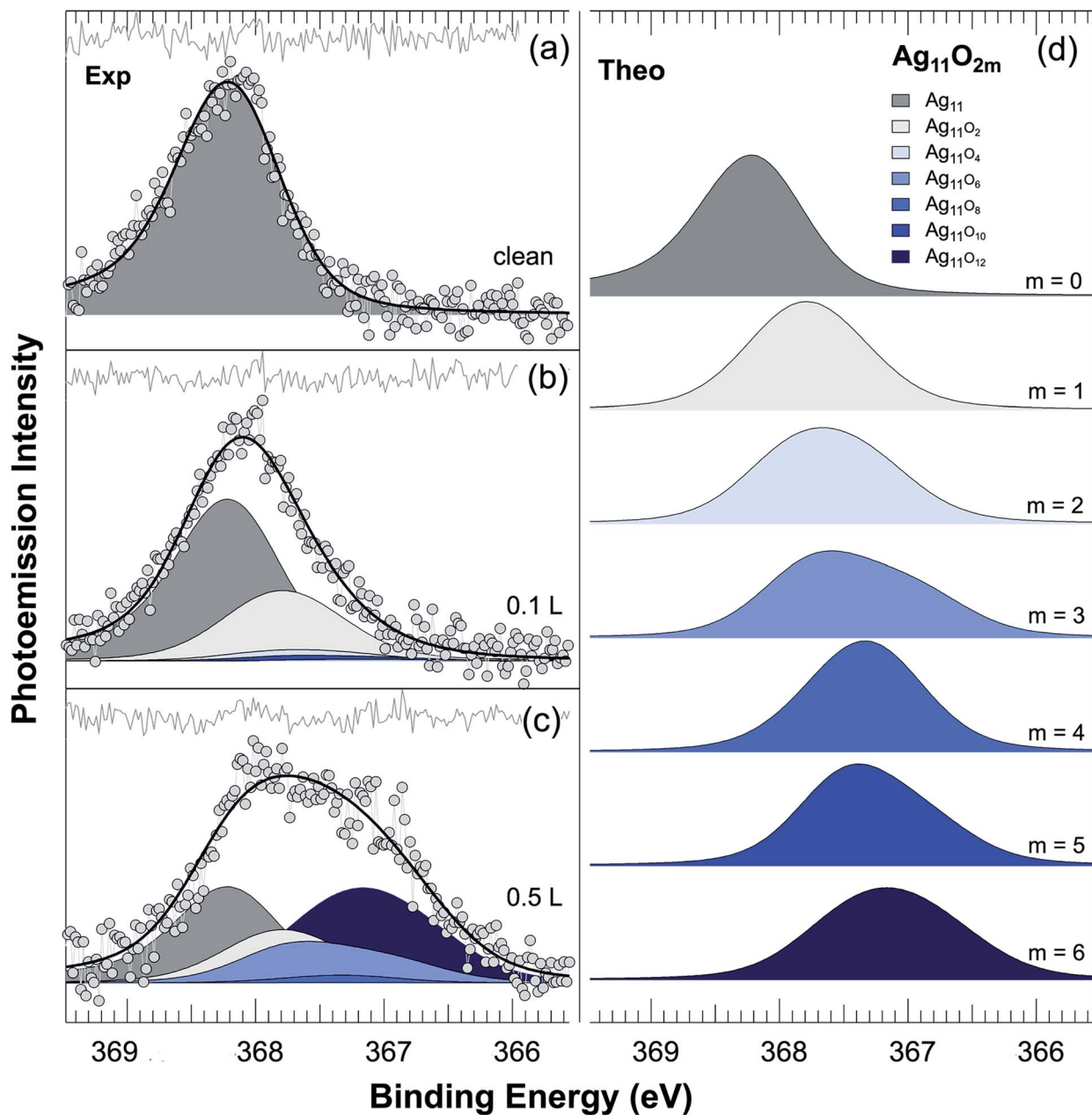


Fig. 2 Experimental Ag $3d_{5/2}$ core level spectra (gray dots) of (a) metallic, (b) mildly- and (c) highly-oxidized Ag_{11} clusters supported on graphene/Ru(0001), fitting lineshape (black line), residuals (gray line) and spectral decomposition (filled areas). (d) DFT-calculated Ag $3d_{5/2}$ core level spectra for each of the $Ag_{11}O_{2m}$ clusters ($m = 0-6$).

calculations were carried out starting from a single Ag_{11} cluster in a complete graphene moiré cell supported by four Ru layers (Fig. 3(a)) to obtain the $3d_{5/2}$ core level binding energies of each Ag atom. The cluster was placed in the valley of the corrugated graphene layer, where we expect stronger interaction with the substrate and a higher stability, as reported for metallic islands grown on Gr/Ru.^{30,66} We found an adsorption energy of the cluster on the Gr/Ru substrate of 2.32 eV, in agreement with the energy obtained for similar Ag clusters on a graphene/SiC substrate.⁶⁷ We used the calculated core-electron binding energies to fit the spectrum in Fig. 2(a) with a Doniach-Šunjić lineshape obtaining a Lorentzian (L) to Gaussian (G) width ratio

of 0.3 : 0.7, a value consistent with a similar study on Ag nanoparticles with diameters below 2 nm,⁶⁷ and an asymmetry parameter $\alpha = 0.09$. The latter is related to the electron density of states at the Fermi energy and to the probability of exciting electron-hole pairs, thus indicating that the metallic character of the cluster is preserved at this scale also. The same DFT calculations were then performed by increasing the number $2m$ of O atoms on the cluster (see Fig. 5S of the ESI†) up to $m = 6$, the minimum oxygen coverage required to fit the experimental data. The Ag $3d_{5/2}$ spectra in Fig. 2(d) were generated by combining the binding energies obtained from the calculations

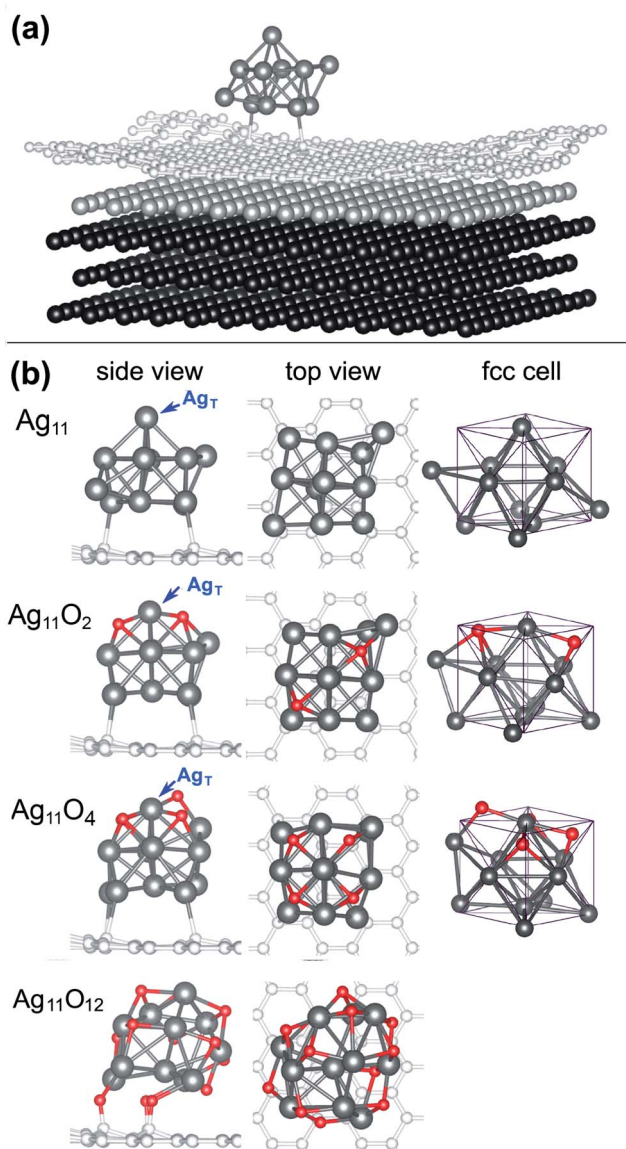


Fig. 3 (a) Super cell used for the calculations including the Ag_{11} nanocluster, a monolayer of graphene supported on 4 layers of Ru describing the Ru(0001) surface. (b) Side and top views and the fcc cell containing the optimized geometry of the Ag_{11} nanocluster obtained by DFT calculations for increasing amounts of oxygen ($m = 0, 1, 2$ and 6). Ag and O are shown in dark grey and red colors, respectively. The Ru atoms in the side and top views are hidden to provide a clearer view of the clusters, but are included in the global cell.

on the Ag $3d_{5/2}$ core levels and preserving the $L : G$ ratio of $0.3 : 0.7$ obtained from the analysis on the clean cluster.

After the first exposure of 0.1 L of O_2 (Fig. 2(b)), a distribution of different $\text{Ag}_{11}\text{O}_{2m}$ clusters appears. The most abundant clusters on the sample are unreacted Ag_{11} (57%) and Ag_{11}O_2 (32%), while the percentage rapidly decreases for Ag_{11}O_4 and Ag_{11}O_6 . $\text{Ag}_{11}\text{O}_{2m}$ clusters with $m > 3$ were then obtained after exposing the clusters to an additional 0.5 L of O_2 (Fig. 2(c)). In this case, the spectral analysis suggests that an Ag : O atomic ratio close to 1 can be reached, with $\text{Ag}_{11}\text{O}_{12}$ representing almost 40% of the total spectral weight. Calculations on the

adsorption energy per oxygen atom (E_b) for each cluster indicate that $\text{Ag}_{11}\text{O}_{12}$ is particularly stable, with a higher E_b of 0.4 eV than that of the neighboring $\text{Ag}_{11}\text{O}_{10}$. This difference can justify the low abundance of $\text{Ag}_{11}\text{O}_{10}$ that emerges from the spectral analysis. A similar trend can be also identified between Ag_{11}O_2 and Ag_{11}O_4 : the latter has a 0.5 eV lower E_b compared to the former and does not give a detectable contribution to the overall spectral weight.

In addition to the effects on the core level binding energies, the oxidation induces relevant structural and electronic modifications in the cluster. To provide a deeper understanding of them, we first focus on the local and global properties of $\text{Ag}_{11}\text{O}_{2m}$ in the low oxygen density region, with $m < 2$ (O/Ag ratio less than 40%). The lowest energy cluster geometry for unreacted Ag_{11} in the gas phase is a triangular prism motif, with five Ag atoms capping their five faces (three squares and two triangles). This configuration is slightly modified after deposition, suggesting that the supporting graphene surface might affect the cluster structure, despite the low interaction of Ag atoms with graphene (see Fig. 6S of the ESI†).

By increasing the number of oxygen atoms, the geometry of $\text{Ag}_{11}\text{O}_{2m}$ changes progressively. In particular, for $m = 1$, the Ag atoms of the cluster assume the configuration of a vertical octahedron with the lower faces capped with 4 Ag atoms, plus an extra Ag (Fig. 3(b)). It is worth discussing in particular the behavior of Ag_T , *i.e.* the silver atom sitting at the top of the cluster, which assumes different configurations upon increasing oxygen adsorption. For $m = 1$, this atom takes part in a O- Ag_T -O linear configuration, which is the typical local geometry of d^{10} Ag(I) ions present in Ag_2O and AgO bulk oxides.⁶⁸ The same linear configuration is obtained even if DFT calculations are performed starting from an initial geometry with two oxygen atoms in adjacent three-fold sites around Ag_T (see the $m = 1$ b panel of Fig. 3S of the ESI†). An O- Ag_T bond length of 2.10 \AA is slightly larger (2.5%) when compared to the experimental findings for Ag_2O bulk systems (2.05 \AA),⁶⁹ but it is consistent with calculations performed with similar DFT formalism.⁶⁸ An average E_b of almost 4.2 eV per atom indicates a rather strong chemisorption.

By increasing the oxygen density ($m = 2$), the cluster shows a quasi-ordered fcc structure. This ordered structure is absolutely uncommon in clusters of this size: it was previously observed only in the kernel of larger protected Ag and Au nanoclusters and nanoparticles, such as Ag_{70} ,⁷⁰ Au_{28} ,⁷¹ Au_{36} ,⁷² *etc.* Moreover, the evident progressive evolution from a triangular-prism structure to a fcc-like cluster with a complete octahedral core could pave the road towards the understanding of the transition from cluster to bulk-like crystalline structures. Most importantly, for $m = 2$, we begin observing the formation of a structural motif that is the basis for the construction of the AgO and Ag_2O_3 bulk silver oxides: a AgO_4 subunit consisting of a d^8 Ag(III) ion possessing an approximate square planar coordination with four O atoms.⁶⁸ This subunit can be found in the Ag_{11}O_4 cluster around Ag_T (see Fig. 3), suggesting that this atom is a d^8 Ag(III) ion. In addition, we found that an average O- Ag_T distance of 2.05 \AA is slightly larger than a bulk value of 2.02 \AA by 1.5%.

To further investigate the resemblance of the local configuration of the cluster with Ag ions in bulk silver oxides, we also studied their electronic properties by calculating the projected density of states (PDOS) of Ag(I), Ag(III) and O ions both in the cluster and in the bulk (Ag_2O and AgO) (see Fig. 4). For $m = 0$, the PDOS of AgT in the metallic state is in agreement with that of similar systems involving Ag atoms and small clusters on graphene,^{73,74} with the d-band confined in the range $E-E_F = -6$ eV to -2.5 eV. Moving to $m = 1$ (Ag_{11}O_2), the PDOS of AgT and Ag(I) in Ag_2O shows large similarities. The Ag 4d and O 2p states dominate the energy range $E-E_F = -7$ eV to -4 eV, with a small contribution coming from the s states, and Ag 4d greatly increases in the range -4 to -2 eV, reaching a maximum at about 3 eV below the Fermi energy for both cluster and bulk Ag_2O . Close to the Fermi energy, the valence band in the energy range -2 eV to 0 eV is a mixture of Ag 4d and O 2p states, with a small contribution coming from Ag 5s, while the conduction band is a mixture of Ag 4d, 5s and 4p states.

We also investigated the electronic distribution through Bader charge analysis to quantify the oxidation state of silver atoms.⁷⁵ Also, in this case, we found out that AgT is very similar to Ag(I) in Ag_2O with a charge difference of only 0.02 e (0.49 e vs. 0.47 e, respectively). The charge distribution per oxygen bond in the cluster is also consistent with the adsorption of atomic O on Ag(111)⁷⁵ and Ag(110)⁷⁶ surfaces. The resemblance with Ag bulk oxides and surfaces corroborates the suggestion of Han and

Jung⁷⁷ that charge localization does not necessarily correlate with superatomic behaviors, but it can provide simple electrostatic explanations.

In the case of the Ag_{11}O_4 cluster, we focus on AgO rather than Ag_2O_3 because the latter only contains Ag(III) ions,⁷⁸ while AgO also contains Ag atoms with a lower oxidation number, thus having a hybrid structure with Ag(III) and Ag(I) atoms bonded respectively to four and two oxygen atoms.⁷⁹ Since AgT is surrounded almost entirely by Ag atoms bonded to 2 oxygen atoms each, we consider that it would be more fruitful to compare Ag_{11}O_4 with the bulk system AgO. This comparison highlighted some similarities between AgT in Ag_{11}O_4 and also the bulk structure from the electronic point of view, as shown by their PDOS (Fig. 4). In particular, the density of states in the energy range -4 to -2 eV greatly decreases when compared to the previous Ag_{11}O_2 cluster and Ag(I) ion, and the bottom of the conduction band is now dominated by a mixture of Ag 4d and O 2p states in the range 0–2 eV.

Further similarities arise from the Bader charge analysis, which gives a comparable result of 0.96 e and 0.99 e for the atom that we identify as a Ag(III) ion in the Ag_{11}O_4 cluster and for Ag(III) in AgO bulk oxide, respectively. The appearance of a Ag(III) atom in the sub-nanometer regime is intriguing, since it co-occurs with a clear breakdown of the superatomic behavior, with a single atom of the cluster reaching a different oxidation state than the others. A complete structural modification of the

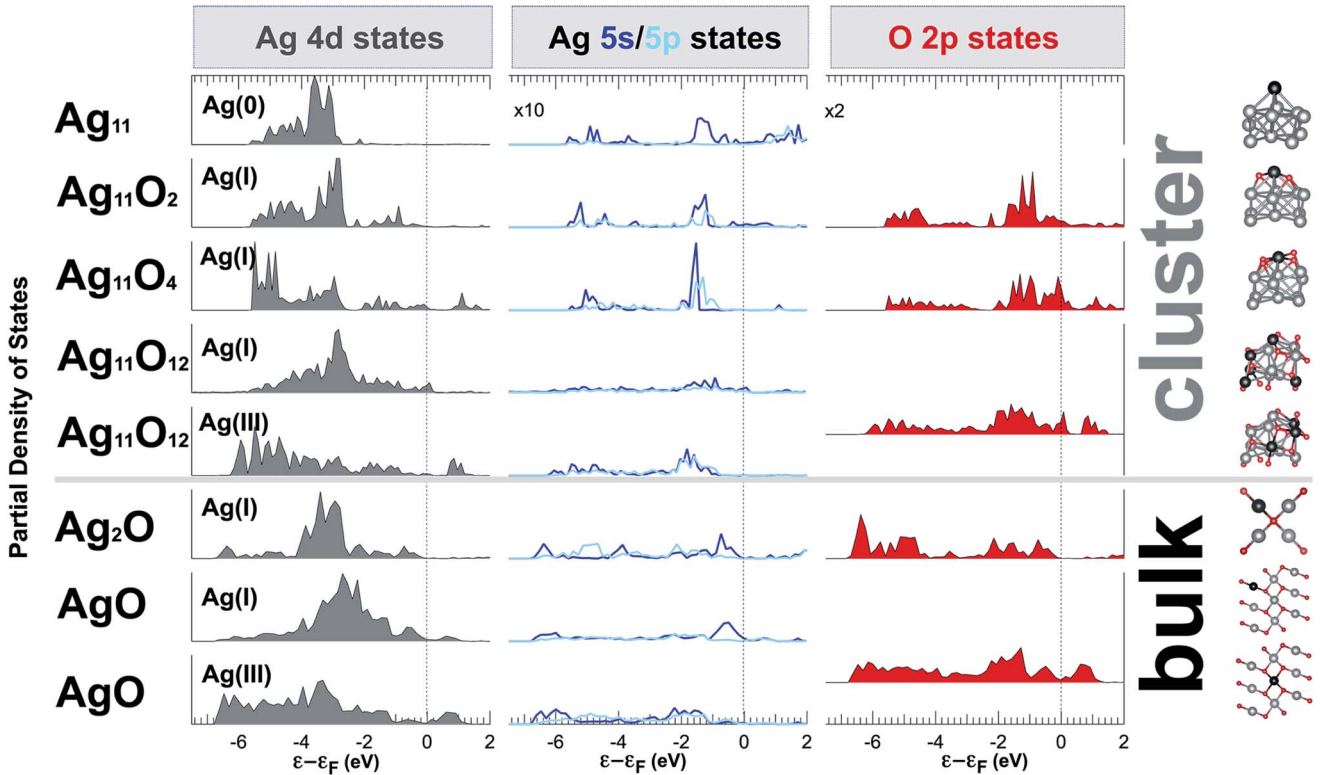


Fig. 4 Calculated PDOS for $\text{Ag}_{11}\text{O}_{2m}$ clusters in different stages of oxidation ($m = 0, 1, 2, 6$). The contributions to the total PDOS from Ag 4d, Ag 5s/5p and O 2p electronic states are reported. The results obtained for bulk Ag_2O and AgO are also reported for comparison. The ball model on the right-hand-side displays the crystalline structure considered for calculations, both for the Ag_{11} nanocluster and bulk-oxide.

cluster is obtained in $\text{Ag}_{11}\text{O}_{12}$, the cluster with the highest amount of oxygen probed in our calculations and the most abundant cluster after the 0.5 L O_2 dose according to our previous analysis. As shown in Fig. 3 (last row), $\text{Ag}_{11}\text{O}_{12}$ presents both Ag atoms forming AgO_4 subunits typical of d^8 Ag(III) ions and in a linear O-Ag-O structure characteristic of Ag(I) ions with d^{10} orbitals, resembling the AgO hybrid bulk oxide structure.^{68,79} This cluster does not have a fcc structure, and the average Ag–Ag bond length increases to 2.94 Å. Moreover, the average Ag–O bond lengths in the cluster are consistent with the experimental findings on AgO : the $\text{Ag(I)}\text{-O}$ and $\text{Ag(III)}\text{-O}$ bond lengths in the bulk are 2.16 Å and 2.03 Å, respectively, *i.e.* very close to the values of 2.17 Å and 2.06 Å obtained for the $\text{Ag}_{11}\text{O}_{12}$ cluster.

In addition to this similarity in the atomic local structure, the electronic structure of $\text{Ag}_{11}\text{O}_{12}$ also strongly resembles that of AgO . In Fig. 4, we plot the calculated Ag 4d, 5p/5s and O 2s PDOS for Ag(I) and Ag(III) atoms for both $\text{Ag}_{11}\text{O}_{12}$ and AgO . A clear difference between the two non-equivalent Ag species can be found in the conduction band maximum, which appears for Ag(III) when the unoccupied 4d states are mixed with the 2p O states, *i.e.*, the same state which was present in the case of lower oxygen density ($m = 2$). Besides this, Ag(I) 4d states are present with higher densities with respect to Ag(III) in the vicinity of the Fermi energy. Same degree of similarities can be appreciated through a quantitative evaluation of the Bader charge in the nanocluster and in the oxide phases. We obtain values of 0.58 e, 0.96 e and -0.77 e, respectively, for Ag(I) , Ag(III) and O atoms in the $\text{Ag}_{11}\text{O}_{12}$ cluster, differing by less than 13% from the values of 0.65 e, 0.99 e and -0.85 e we find for the same atoms in the AgO bulk oxide. This outcome can be compared with those arising from the longstanding investigations of the oxidation process on single crystal silver surfaces. The local low O density configuration corresponding to $m = 2$ is very similar to that observed in the case of Ag(110) , for which the surface reconstructs with a $p(2 \times 1)$ periodicity according to the missing row model and also shows a Ag $3d_{5/2}$ core level shift of -0.4 eV,⁸⁰ in agreement with the outcomes of this work. However, according to DFT calculations, this local configuration does not play any role in the important epoxidation reaction.⁸¹ Quite remarkably, for higher oxygen densities, for which atomic oxygen is known to induce large structural modifications on Ag solid surfaces, especially on Ag(111) , most of the oxide structures that appear do not present the local AgO_4 arrangement similar to what we have found. In particular, every structure that has been proposed to describe the $p(4 \times 4)$ phase on Ag(111) , which was considered for a long time to be the configuration that ensures the unique properties of Ag towards the epoxidation reaction and has only recently been ruled out, turns out to be totally dissimilar from our findings. The same is true for the $p(4 \times 5\sqrt{3})\text{rect}$, $c(3 \times 5\sqrt{3})\text{rect}$ and $p(7 \times 7)$ phases which have been deeply investigated by means of several experimental techniques.^{82–85} The only structure proposed which presents a local arrangement similar to the one we have found at the nanoscale is the $c(4 \times 8)$ phase, which corresponds to an oxygen coverage of 0.5 ML with two nonequivalent Ag atoms (α and β type) that show core level shifts of -0.9 and -0.5 eV, respectively. Interestingly, the α type Ag configuration with the first layer silver atoms surrounded by 4 oxygen atoms presents the

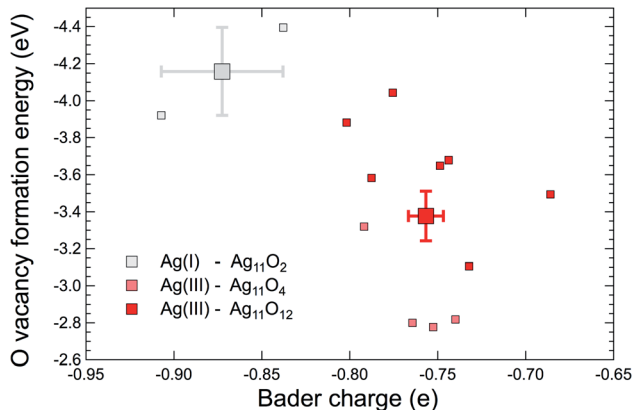


Fig. 5 Calculated oxygen vacancy formation energy for different configuration in the Ag_{11}O_2 , Ag_{11}O_4 and $\text{Ag}_{11}\text{O}_{12}$ clusters. Grey and red squares correspond to O atoms bonded to Ag(III) and Ag(I) atoms, respectively. Large squares are the average of the single values.

larger and negative $3d_{5/2}$ core level shift, as in our case. However, contrary to the case of solid surfaces, where all the different ordered surface oxide structures present a similar energetic stability, the local configuration we found appears already for low Ag:O ratios. Notably, this model has been only recently confirmed by state-of-the-art simulations based on the atomistic structure learning algorithm developed for structural determination in combination with first-principles total energy calculations.⁸⁶

Besides the appearance of bulk-like structural motifs at the nanoscale, the results discussed in the present work could also have implications in terms of chemical reactions, more specifically for the silver epoxidation reaction, which is extremely relevant from a technological point of view, but it relies on a mechanism not fully understood yet. In order to address this issue, we have calculated the oxygen vacancy formation energy EO_{vac} , which is an important parameter in determining the chemical reactivity of metal oxide, as a function of the oxygen content and configuration in the nanocluster. EO_{vac} can be used, as a matter of fact, to predict the trend of catalytic performance.⁸⁷ Fig. 5 shows the relationship between EO_{vac} and the Bader charge for different oxygen atoms belonging to clusters at low ($m = 1$), intermediate ($m = 2$) and high O densities ($m = 6$). The local configuration of vacancy formation is, for $m = 1$, to the one occupied by oxygen atoms bonded with only Ag(I) atoms (light gray squares in Fig. 5), whereas for $m = 2$ and $m = 6$, the bond is formed with at least the Ag(III) species (dark gray squares in Fig. 5). It is clear that the average EO_{vac} (large squares) is favored by approx. 0.8 eV in the case of the $\text{Ag(III)}\text{-O}$ bond, *i.e.* for those O atoms which present a larger Bader charge.

4 Conclusions

The appearance of distinctive bulk features for clusters of few atoms in the sub-nanometer regime emerges as a peculiar behavior of nano-oxides, and it is not observed for metallic clusters²¹ or clusters of other elements, such as boron,⁸⁸ silicon,^{89,90} and carbon.⁹¹ For Ag atoms, few tens of atoms are

required to observe the shift towards bulk-like configurations, while in specific situations, the presence of internal strain could also result in an unexpected and stable body-centred tetragonal phase in Ag nanoparticles.⁹² Other oxide clusters have been reported to display bulk-related configurations already at this small size, as for molybdenum and tungsten cluster oxide, for which the cluster configuration and morphology are comparable to those of their parent bulk counterpart. Bondarchuk *et al.* report $(\text{WO}_3)_n$ clusters, with $n = 1-4$, that are produced by WO_3 powder sublimation and show a local geometry in the shape of a triangle whose sides are arranged in the O-W-O fashion.⁹³ Theoretical calculations indicate that this feature is already expected from the bulk oxide. However, it has to be stressed that, unlike WO_3 clusters, the Ag oxide clusters we prepared are not produced by fragmentation of a bulk oxide crystal, where the building blocks present at the macroscopic scale are separated through a process of thermal excitation while retaining their structural identity. On the contrary, our results show that 3D motifs can also be obtained through a chemical oxidation process starting from a nanoscale material that initially is in a metallic state, with potential implications in the atomically precise design of sub-nano catalysts^{94,95}

Besides the process that leads to the formation of the oxidized cluster in this peculiar conformation, it is important to emphasize the importance of the presence of two non-equivalent species of Ag atoms, which can be instrumental to the use of this type of cluster in bifunctional catalysis processes. We can expect that the different electron charge densities existing in Ag(I) and Ag(III) would largely modify the atomic and molecular adsorption capacities on the respective adsorption sites. Moreover, the presence of two functional groups could result in a cooperative effect capable of bringing different levels of catalytic efficiency and selectivity in specific chemical reactions. In addition, the Ag oxide clusters studied in our experiment also have unique features in view of their importance for the epoxidation reaction, for which Ag has a vast range of applications. This reaction requires two crucial ingredients: (i) the need of an oxygen rich surface with weak O-surface bonding and (ii) the presence of cationic atoms that can inhibit the dehydrogenation reaction channel.⁸¹ Both conditions are satisfied in the structure we found for the $\text{Ag}_{11}\text{O}_{12}$ cluster, whilst this is not the case for single crystal Ag surfaces.

The presence of bulk-like local configuration supports the fact that matter at the nanoscale behaves in a different way with respect to the widely-investigated world of solid surfaces. Our achievement could have important implications in the use of atomic clusters for chemical reactions, in particular, for the epoxidation of ethylene, for which Ag has a vast range of applications. We believe that these results could be instrumental to lay the foundations for new and more efficient use of Ag in catalysts in the form of sub-nanometer Ag oxide clusters.

Author contributions

A. B. conceived the project and coordinated the research activities. A. K., U. H. and A. B. designed the cluster source. F. L., L. S. and L. B. performed the set-up of the cluster source and performed the deposition. P. L. and S. L. performed the set-up of

the SuperESCA beamline. F. L., L. B., L. B., P. L., E. T., S. L. and A. B. performed the X-ray photoelectron spectroscopy measurements. F. L. carried out the experimental data analysis. M. P. and D. A. carried out the density functional theory calculations. F. L., L. B. and A. B. wrote the manuscript. All authors extensively discussed the results and the interpretation and revised the manuscript.

Conflicts of interest

There are no conflicts to declare.

Acknowledgements

We acknowledge funding from the University of Trieste through the METAMAT project. L. B. acknowledges funding from the University of Trieste through the D55 Microgrants funding initiative. M. P. and D. A. are supported by the Natural Environment Research Council (grant No. NE/R000425/1). DFT calculations were performed on the Monsoon2 system, a collaborative facility supplied under the Joint Weather and Climate Research Programme, a strategic partnership between the UK Met Office and the Natural Environment Research Council.

References

- 1 W. Huang, *Acc. Chem. Res.*, 2016, **49**, 520–527.
- 2 C. L. Cleveland, U. Landman, T. G. Schaaff, M. N. Shafiqullin, P. W. Stephens and R. L. Whetten, *Phys. Rev. Lett.*, 1997, **79**, 1873.
- 3 J. Li, X. Li, H.-J. Zhai and L.-S. Wang, *Science*, 2003, **299**, 864–867.
- 4 T. L. Christiansen, E. D. Bøjesen, M. Juelsholt, J. Etheridge and K. M. Ø. Jensen, *ACS Nano*, 2019, **13**, 8725–8735.
- 5 A. Desireddy, B. E. Conn, J. Guo, B. Yoon, R. N. Barnett, B. M. Monahan, K. Kirschbaum, W. P. Griffith, R. L. Whetten, U. Landman, *et al.*, *Nature*, 2013, **501**, 399–402.
- 6 D. Chen and J. Li, *Nanoscale Horiz.*, 2020, **5**, 1355–1367.
- 7 Z. Wang, B. Chen and A. L. Rogach, *Nanoscale Horiz.*, 2017, **2**, 135–146.
- 8 K. G. Stamplecoskie and A. Swint, *J. Mater. Chem. A*, 2016, **4**, 2075–2081.
- 9 J. U. Reveles, P. A. Clayborne, A. C. Reber, S. N. Khanna, K. Pradhan, P. Sen and M. R. Pederson, *Nat. Chem.*, 2009, **1**, 310–315.
- 10 X. Zhang, Y. Wang, H. Wang, A. Lim, G. Gantefoer, K. H. Bowen, J. U. Reveles and S. N. Khanna, *J. Am. Chem. Soc.*, 2013, **135**, 4856–4861.
- 11 Y.-J. Ko, K. Choi, B. Yang, W. H. Lee, J.-Y. Kim, J.-W. Choi, K. H. Chae, J. H. Lee, Y. J. Hwang, B. K. Min, H.-S. Oh and W.-S. Lee, *J. Mater. Chem. A*, 2020, **8**, 9859–9870.
- 12 Y. Lei, F. Mehmood, S. Lee, J. Greeley, B. Lee, S. Seifert, R. E. Winans, J. W. Elam, R. J. Meyer, P. C. Redfern, D. Teschner, R. Schlögl, M. J. Pellin, L. A. Curtiss and S. Vajda, *Science*, 2010, **328**, 224–228.

- 13 E. C. Tyo and S. Vajda, *Nat. Nanotechnol.*, 2015, **10**, 577–588.
- 14 L. Liu and A. Corma, *Chem. Rev.*, 2018, **118**, 4981–5079.
- 15 R. Wang, D. Li, S. Maurya, Y. S. Kim, Y. Wu, Y. Liu, D. Strmcnik, N. M. Markovic and V. R. Stamenkovic, *Nanoscale Horiz.*, 2019, **5**, 316–324.
- 16 C. Yin, F. R. Negreiros, G. Barcaro, A. Beniya, L. Sementa, E. C. Tyo, S. Bartling, K.-H. Meiwes-Broer, S. Seifert, H. Hirata, N. Isomura, S. Nigam, C. Majumder, Y. Watanabe, A. Fortunelli and S. Vajda, *J. Mater. Chem. A*, 2017, **5**, 4923–4931.
- 17 T. Chen, L. Ye and T. W. B. Lo, *J. Mater. Chem. A*, 2021, **9**, 18773–18784.
- 18 J.-F. Huang, R.-H. Zeng and J.-L. Chen, *J. Mater. Chem. A*, 2021, **9**, 21972–21980.
- 19 J. Cai, R. Javed, D. Ye, H. Zhao and J. Zhang, *J. Mater. Chem. A*, 2020, **8**, 22467–22487.
- 20 T. Kawawaki, Y. Kataoka, M. Hirata, Y. Iwamatsu, S. Hossain and Y. Negishi, *Nanoscale Horiz.*, 2021, **6**, 409–448.
- 21 F. Baletto and R. Ferrando, *Rev. Mod. Phys.*, 2005, **77**, 371.
- 22 S. Ulstrup, P. Lacovig, F. Orlando, D. Lizzit, L. Bignardi, M. Dalmiglio, M. Bianchi, F. Mazzola, A. Baraldi, R. Larciprete, P. Hofmann and S. Lizzit, *Surf. Sci.*, 2018, **678**, 57–64.
- 23 D. Alfè, M. Pozzo, E. Miniussi, S. Günther, P. Lacovig, S. Lizzit, R. Larciprete, B. S. Burgos, T. O. Menteş, A. Locatelli and A. Baraldi, *Sci. Rep.*, 2013, **3**, 2430.
- 24 U. Heiz, F. Vanolli, L. Trento and W.-D. Schneider, *Rev. Sci. Instrum.*, 1997, **68**, 1986–1994.
- 25 L. Sbuelz, F. Loi, M. Pozzo, L. Bignardi, E. Nicolini, P. Lacovig, E. Tosi, S. Lizzit, A. Kartouzian, U. Heiz, *et al.*, *J. Phys. Chem. C*, 2021, **125**, 9556–9563.
- 26 C. Binns, *Surf. Sci. Rep.*, 2001, **44**, 1–49.
- 27 S. J. Carroll, P. Weibel, B. von Issendorff, L. Kuipers and R. E. Palmer, *J. Phys.: Condens. Matter*, 1996, **8**, L617–L624.
- 28 S. Doniach and M. Sunjic, *J. Phys. C: Solid State Phys.*, 1970, **3**, 285.
- 29 G. Kresse and J. Furthmüller, *Phys. Rev. B: Condens. Matter Mater. Phys.*, 1996, **54**, 11169.
- 30 P. J. Feibelman, *Phys. Rev. B: Condens. Matter Mater. Phys.*, 2008, **77**, 165419.
- 31 I. Hamada, *Phys. Rev. B: Condens. Matter Mater. Phys.*, 2014, **89**, 121103.
- 32 P. E. Blöchl, *Phys. Rev. B: Condens. Matter Mater. Phys.*, 1994, **50**, 17953.
- 33 J. P. Perdew, K. Burke and M. Ernzerhof, *Phys. Rev. Lett.*, 1996, **77**, 3865.
- 34 W. Knight, K. Clemenger, W. A. de Heer, W. A. Saunders, M. Chou and M. L. Cohen, *Phys. Rev. Lett.*, 1984, **52**, 2141.
- 35 C. Yannouleas and U. Landman, in *Recent Progress in Orbital-free Density Functional Theory*, World Scientific, Singapore, 2012, ch. 7, pp. 203–249.
- 36 G. U. Gamboa, A. C. Reber and S. N. Khanna, *New J. Chem.*, 2013, **37**, 3928–3935.
- 37 J. Zhao, Y. Luo and G. Wang, *Eur. Phys. J. D*, 2001, **14**, 309–316.
- 38 J. Li and C.-y. Liu, *Eur. J. Inorg. Chem.*, 2010, **2010**, 1244–1248.
- 39 I. Lado-Touriño and A. Páez-Pavón, *Nanomaterials*, 2021, **11**, 1378–1393.
- 40 M. Al-Hada, S. Peters, L. Gregoratti, M. Amati, H. Sezen, P. Parisse, S. Selve, T. Niermann, D. Berger, M. Neeb, *et al.*, *Surf. Sci.*, 2017, **665**, 108–113.
- 41 R. Dietsche, D. C. Lim, M. Bubek, I. Lopez-Salido, G. Ganteför and Y. D. Kim, *Appl. Phys. A: Mater. Sci. Process.*, 2008, **90**, 395–398.
- 42 Z. Zhou, F. Gao and D. W. Goodman, *Surf. Sci.*, 2010, **604**, L31–L38.
- 43 X. Liu, C.-Z. Wang, M. Hupalo, W. Lu, M. C. Tringides, Y. Yao and K.-M. Ho, *Phys. Chem. Chem. Phys.*, 2012, **14**, 9157–9166.
- 44 X. Liu, Y. Han, J. W. Evans, A. K. Engstfeld, R. J. Behm, M. C. Tringides, M. Hupalo, H.-Q. Lin, L. Huang, K.-M. Ho, *et al.*, *Prog. Surf. Sci.*, 2015, **90**, 397–443.
- 45 R. T. Frederick, Z. Novotny, F. P. Netzer, G. S. Herman and Z. Dohnalek, *J. Phys. Chem. B*, 2018, **122**, 640–648.
- 46 D. Martoccia, P. Willmott, T. Brugger, M. Björck, S. Günther, C. Schlepütz, A. Cervellino, S. Pauli, B. Patterson, S. Marchini, *et al.*, *Phys. Rev. Lett.*, 2008, **101**, 126102.
- 47 B. F. Habenicht, D. Teng, L. Semidey-Flecha, D. S. Sholl and Y. Xu, *Top. Catal.*, 2014, **57**, 69–79.
- 48 M. M. Montemore, M. A. van Spronsen, R. J. Madix and C. M. Friend, *Chem. Rev.*, 2017, **118**, 2816–2862.
- 49 Y. Xu, J. Greeley and M. Mavrikakis, *J. Am. Chem. Soc.*, 2005, **127**, 12823–12827.
- 50 I. Lončarić, M. Alducin and J. Juaristi, *Phys. Chem. Chem. Phys.*, 2015, **17**, 9436–9445.
- 51 S. Klacar, A. Hellman, I. Panas and H. Gronbeck, *J. Phys. Chem. C*, 2010, **114**, 12610–12617.
- 52 C. Sprodownski, M. Mehlhorn and K. Morgenstern, *J. Phys.: Condens. Matter*, 2010, **22**, 264005.
- 53 P. Jiang, S. Porsgaard, F. Borondics, M. Köber, A. Caballero, H. Bluhm, F. Besenbacher and M. Salmeron, *J. Am. Chem. Soc.*, 2010, **132**, 2858–2859.
- 54 M. Larsson, P. Baltzer, S. Svensson, B. Wannberg, N. Martensson, A. N. de Brito, N. Correia, M. Keane, M. Carlsson-Gothe and L. Karlsson, *J. Phys. B: At., Mol. Opt. Phys.*, 1990, **23**, 1175.
- 55 R. Larciprete, S. Fabris, T. Sun, P. Lacovig, A. Baraldi and S. Lizzit, *J. Am. Chem. Soc.*, 2011, **133**, 17315–17321.
- 56 Z. Novotny, M.-T. Nguyen, F. P. Netzer, V.-A. Glezakou, R. Rousseau and Z. Dohnalek, *J. Am. Chem. Soc.*, 2018, **140**, 5102–5109.
- 57 M. Wagstaffe, H. Hussain, M. J. Acres, R. Jones, K. L. Syres and A. G. Thomas, *J. Phys. Chem. C*, 2017, **121**, 21383–21389.
- 58 C. Heine, B. Eren, B. A. Lechner and M. Salmeron, *Surf. Sci.*, 2016, **652**, 51–57.
- 59 M. E. Turano, R. G. Farber, E. C. Oskorep, R. A. Rosenberg and D. R. Killelea, *J. Phys. Chem. C*, 2019, **124**, 1382–1389.
- 60 J. Schnadt, A. Michaelides, J. Knudsen, R. T. Vang, K. Reuter, E. Lægsgaard, M. Scheffler and F. Besenbacher, *Phys. Rev. Lett.*, 2006, **96**, 146101.
- 61 M. Schmid, A. Reicho, A. Stierle, I. Costina, J. Klikovits, P. Kostelnik, O. Dubay, G. Kresse, J. Gustafson, E. Lundgren, *et al.*, *Phys. Rev. Lett.*, 2006, **96**, 146102.

- 62 M. Gajdoš, A. Eichler and J. Hafner, *Surf. Sci.*, 2003, **531**, 272–286.
- 63 T. C. Kaspar, T. Droubay, S. A. Chambers and P. S. Bagus, *J. Phys. Chem. C*, 2010, **114**, 21562–21571.
- 64 G. N. Vayssilov, Y. Lykhach, A. Migani, T. Staudt, G. P. Petrova, N. Tsud, T. Skála, A. Bruix, F. Illas, K. C. Prince, *et al.*, *Nat. Mater.*, 2011, **10**, 310–315.
- 65 M. Al-Hada, L. Gregoratti, M. Amati and M. Neeb, *Surf. Sci.*, 2020, **693**, 121533.
- 66 B. F. Habenicht, D. Teng, L. Semidey-Flecha, D. S. Sholl and Y. Xu, *Top. Catal.*, 2014, **57**, 69–79.
- 67 I. Shtepliuk and R. Yakimova, *ACS Omega*, 2021, **6**, 24739–24751.
- 68 J. P. Allen, D. O. Scanlon and G. W. Watson, *Phys. Rev. B: Condens. Matter Mater. Phys.*, 2011, **84**, 115141.
- 69 P. Norby, R. Dinnebier and A. N. Fitch, *Inorg. Chem.*, 2002, **41**, 3628–3637.
- 70 Y.-M. Su, Z. Wang, G.-L. Zhuang, Q.-Q. Zhao, X.-P. Wang, C.-H. Tung and D. Sun, *Chem. Sci.*, 2019, **10**, 564–568.
- 71 C. Zeng, T. Li, A. Das, N. L. Rosi and R. Jin, *J. Am. Chem. Soc.*, 2013, **135**, 10011–10013.
- 72 C. Zeng, H. Qian, T. Li, G. Li, N. L. Rosi, B. Yoon, R. N. Barnett, R. L. Whetten, U. Landman and R. Jin, *Angew. Chem., Int. Ed.*, 2012, **51**, 13114–13118.
- 73 M. R. Mananghaya, G. N. Santos and D. Yu, *Org. Electron.*, 2018, **63**, 355–361.
- 74 R. M. Del Castillo and L. E. Sansores, *Eur. Phys. J. B*, 2015, **88**, 248.
- 75 V. I. Bukhtiyarov, M. Hävecker, V. V. Kaichev, A. Knop-Gericke, R. W. Mayer and R. Schlögl, *Phys. Rev. B: Condens. Matter Mater. Phys.*, 2003, **67**, 235422.
- 76 T. B. Rawal, S. Hong, A. Pulkkinen, M. Alatalo and T. S. Rahman, *Phys. Rev. B: Condens. Matter Mater. Phys.*, 2015, **92**, 035444.
- 77 Y.-K. Han and J. Jung, *J. Am. Chem. Soc.*, 2008, **130**, 2–3.
- 78 B. Standke and M. Jansen, *Angew. Chem., Int. Ed.*, 1985, **24**, 118–119.
- 79 J. P. Allen, D. O. Scanlon and G. W. Watson, *Phys. Rev. B: Condens. Matter Mater. Phys.*, 2010, **81**, 161103.
- 80 T. E. Jones, R. Wyrwich, S. Böcklein, T. C. Rocha, E. A. Carbonio, A. Knop-Gericke, R. Schlögl, S. Günther, J. Wintterlin and S. Piccinin, *J. Phys. Chem. C*, 2016, **120**, 28630–28638.
- 81 D. Chen, P.-L. Kang and Z.-P. Liu, *ACS Catal.*, 2021, **11**, 8317–8326.
- 82 N. M. Martin, S. Klacar, H. Grönbeck, J. Knudsen, J. Schnadt, S. Blomberg, J. Gustafson and E. Lundgren, *J. Phys. Chem.*, 2014, **118**, 15324–15331.
- 83 M. E. Turano, L. B. F. Juurlink, M. Z. Gillum, E. A. Jamka, G. Hildebrandt, F. Lewis and D. R. Killelea, *J. Vac. Sci. Technol.*, 2021, **39**, 053201.
- 84 M. E. Turano, R. G. Farber, E. C. N. Oskorep, R. A. Rosenberg and D. R. Killelea, *J. Phys. Chem. C*, 2020, **124**, 1382–1389.
- 85 J. Derouin, R. G. Farber, M. E. Turano, E. V. Iski and D. R. Killelea, *ACS Catal.*, 2016, **6**, 4640–4646.
- 86 H. L. Mortensen, S. A. Meldgaard, M. K. Bisbo, M.-P. V. Christiansen and B. Hammer, *Phys. Rev. B*, 2020, **102**, 075427.
- 87 D. Widmann and R. J. Behm, *Acc. Chem. Res.*, 2014, **47**, 740–749.
- 88 H.-J. Zhai, Y.-F. Zhao, W.-L. Li, Q. Chen, H. Bai, H.-S. Hu, Z. A. Piazza, W.-J. Tian, H.-G. Lu, Y.-B. Wu, Y.-W. Mu, G.-F. Wei, Z.-P. Liu, J. Li, S.-D. Li and L.-S. Wang, *Nat. Chem.*, 2014, **6**, 727–731.
- 89 P. Mélinon, B. Masenelli, F. Tournus and A. Perez, *Nat. Mater.*, 2007, **6**, 479–490.
- 90 U. Röthlisberger, W. Andreoni and M. Parrinello, *Phys. Rev. Lett.*, 1994, **72**, 665.
- 91 W. David, R. Ibberson, J. Matthewman, K. Prassides, T. Dennis, J. Hare, H. Kroto, R. Taylor and D. Walton, *Nature*, 1991, **353**, 147–149.
- 92 Y. Sun, Y. Ren, Y. Liu, J. Wen, J. S. Okasinski and D. J. Miller, *Nat. Commun.*, 2012, **3**, 971.
- 93 O. Bondarchuk, X. Huang, J. Kim, B. D. Kay, L. Wang, J. M. White and Z. Dohnálek, *Angew. Chem., Int. Ed.*, 2006, **45**, 4786–4789.
- 94 S. Mitchell and J. Pérez-Ramírez, *Nat. Rev. Mater.*, 2021, **6**, 969–985.
- 95 S. Mitchell, R. Qin, N. Zheng and J. Pérez-Ramírez, *Nat. Nanotechnol.*, 2021, **16**, 129–139.